Acid-sensing ion channel (ASIC) 1a/2a heteromers have a flexible 2:1/1:2 stoichiometry

Tudor Bartoi[a,b,1], Katrin Augustinowski[c,1], Georg Polleichtner[c], Stefan Gründer[c,2,3], and Maximilian H. Ulbrich[a,b,2,3]

[a]Institute of Physiology II and [b]BIOSS Centre for Biological Signalling Studies, University of Freiburg, 79104 Freiburg, Germany; and [c]Institute of Physiology, Rheinisch-Westfälische Technische Hochschule Aachen University, 52074 Aachen, Germany

Edited by Richard W. Aldrich, The University of Texas at Austin, Austin, TX, and approved April 29, 2014 (received for review December 28, 2013)

Acid-sensing ion channels (ASICs) are widely expressed proton-gated Na^+ channels playing a role in tissue acidosis and pain. A trimeric composition of ASICs has been suggested by crystallization. Upon coexpression of ASIC1a and ASIC2a in *Xenopus* oocytes, we observed the formation of heteromers and their coexistence with homomers by electrophysiology, but could not determine whether heteromeric complexes have a fixed subunit stoichiometry or whether certain stoichiometries are preferred over others. We therefore imaged ASICs labeled with green and red fluorescent proteins on a single-molecule level, counted bleaching steps from GFP and colocalized them with red tandem tetrameric mCherry for many individual complexes. Combinatorial analysis suggests a model of random mixing of ASIC1a and ASIC2a subunits to yield both 2:1 and 1:2 ASIC1a:ASIC2a heteromers together with ASIC1a and ASIC2a homomers.

single-molecule imaging | subunit counting | BLINaC | ENaC

Acid-sensing ion channels (ASICs) are proton-gated Na^+ channels, which are probably ubiquitously expressed in neurons, yet surprisingly little is known about their physiological function in the brain (1). It is believed that ASICs localize to the postsynapse and carry an excitatory postsynaptic current (2). ASICs in central neurons are mainly composed of homomeric ASIC1a and heteromeric ASIC1a/2a (3–6) and ASIC1a/2b (7). Genetic ablation of ASIC1a has indeed led to the conclusion that ASICs contribute to long-term potentiation and memory formation (2), but a more recent study challenged these findings (8). In contrast to our incomplete understanding of the physiological functions of ASICs, there is a comparatively large body of evidence that activation of ASIC1a-containing channels in pathophysiological states that are associated with sustained acidosis contributes to neuronal or axonal degeneration (9, 10). In addition, blockade of the ASIC1a/2a heteromer causes central analgesia (11). Together, these findings render ASIC1a-containing channels attractive drug target candidates.

The crystal structure of chicken ASIC1 revealed an acidic pocket at subunit interfaces, which has been proposed to be the ligand-binding site of ASICs (12). In agreement, it has recently been shown that a gating modifier toxin of ASIC1, psalmotoxin 1, which behaves like an agonist (13), binds at the acidic pocket at subunit interfaces (14–16). Therefore, knowing the subunit composition of the ASIC1a/2a heteromer is of major interest, in particular for pharmacologically targeting this subtype.

Fluorescence resonance energy transfer analysis suggested that the ASIC1a/2a heteromer contains at least two ASIC1a and two ASIC2a subunits (17). In agreement, several studies reported that the related epithelial Na^+ channel (ENaC) is composed of four (18–21) or nine subunits (22–24). In strong contrast, however, the crystal structure of chicken ASIC1 revealed a number of three subunits (12, 25), suggesting that all ASICs and their relatives like ENaC are trimers. The trimeric structure of ASIC1a has in the meanwhile been confirmed by atomic force microscopy imaging (26). The stoichiometry of heteromeric ASICs, however, remains completely unknown.

In this study, we first used electrophysiology to characterize mixtures of ASIC1a and ASIC2a at different expression ratios in *Xenopus laevis* oocytes to demonstrate that at least one heteromeric channel forms. Because we were unable to decide on the existence of a second heteromeric species by electrophysiology, we used a single-molecule photobleaching approach that resolves stoichiometries of membrane proteins with high accuracy. We tagged ASIC1a and ASIC2a with green and red fluorescent reporter proteins, which did not change the electrophysiological characteristics of homo- and heteromeric ASICs, suggesting that fusion of a fluorescent reporter has no impact on the molecular composition of ASICs. Colocalization of red and green reporter tags on a single-molecule level and counting of green bleaching steps confirms the trimeric nature of functional ASICs and shows that ASIC1a and ASIC2a randomly assemble into a complex with a flexible stoichiometry of either 1:2 or 2:1.

Results

Increasing Levels of ASIC2a Progressively Shift the Apparent Proton Affinities of Heteromeric ASIC1a/2a. Using a two-electrode voltage clamp in *Xenopus* oocytes, we characterized the electrophysiological properties of homomeric ASIC1a and homomeric ASIC2a. Transient H^+-gated inward currents carried by ASIC1a completely desensitized at pH 5.7, had a high H^+ affinity with saturating current amplitudes at pH $\leq$ 6.0 and half-maximal activation (pH_{50}) at pH 6.5 $\pm$ 0.1, and a steep concentration–response curve with a Hill coefficient of 3.7, properties typical for ASIC1a (Fig. 1*A*, Fig. S1*A*, and Table S1). H^+-gated inward currents from ASIC2a had clearly different typical properties: incomplete desensitization after 10 s, a

Significance

Our work concerns the stoichiometry of acid-sensing ion channels (ASICs), proton-gated Na^+ channels. In the central nervous system ASICs are composed of either only ASIC1a subunits or ASIC1a and ASIC2a subunits. Blockade of the ASIC1a/2a heteromer causes strong analgesia. Because ligands and drugs bind at subunit interfaces of ASICs, knowing the exact stoichiometry of heteromeric ASICs is pivotal for an informed drug design. We used a single-molecule method where we image individual ion channels that we fused to fluorescent proteins to clearly demonstrate that ASICs assemble into trimers and that coexpression of ASIC1a and ASIC2a leads to a mix of ASIC1a and ASIC2a homomers and ASIC1a:ASIC2a heteromers. Heteromers assemble randomly in both 1:2 and 2:1 compositions.

Author contributions: S.G. and M.H.U. designed research; T.B., K.A., G.P., and M.H.U. performed research; T.B., K.A., G.P., S.G., and M.H.U. analyzed data; and S.G. and M.H.U. wrote the paper.

The authors declare no conflict of interest.

This article is a PNAS Direct Submission.

[1]T.B. and K.A. contributed equally to this work.

[2]S.G. and M.H.U. contributed equally to this work.

[3]To whom correspondence may be addressed. E-mail: max.ulbrich@physiologie.uni-freiburg.de or sgruender@ukaachen.de.

This article contains supporting information online at www.pnas.org/lookup/suppl/doi:10.1073/pnas.1324060111/-/DCSupplemental.

low H^+ affinity with currents appearing only at pH ≤ 5.5, a pH_{50} of ~3.9, and a Hill coefficient of 1.0 (Fig. 1*A*, Fig. S1*A*, and Table S1).

Coexpression of ASIC1a and ASIC2a yielded channels with a continuum of apparent proton affinities, depending on the ratio of the two cRNAs injected. We fitted the apparent H^+ affinity (pH_{50}) with a single Hill function (Fig. 1*B* and Table S1). ASICs at a cRNA ratio of 1:1 had a pH_{50} of 5.6 ± 0.1 ($n = 7$). Increasing the amount of ASIC2a cRNA relative to ASIC1a cRNA (ratio 5:1) slightly shifted pH_{50} to 5.2 ± 0.1 ($n = 6$, $P = 0.02$), and further increasing the amount of ASIC2a cRNA (ratio 15:1) shifted pH_{50} to 5.1 ± 0.0 ($n = 7$, $P < 0.01$). These pH_{50} values are in-between the pH_{50} of the homomeric ASICs and characteristic for heteromeric ASIC1a/2a (27). Only at a cRNA ratio of 25:1 did pH_{50} become ~3, closely resembling homomeric ASIC2a. Moreover, at the 25:1 ratio, channels did not completely desensitize within 10 s at any pH tested and current amplitude strongly increased at pH < 4.5 (Fig. S1*B*), suggesting that homomeric ASIC2a was the main ASIC population.

To test whether the concentration–response curves could originate without the contribution of heteromeric channels, we fitted them with a linear combination of the response curves for homomeric ASIC1a and ASIC2a that we measured initially (Fig. S2). Only for the 25:1 cRNA injection ratio, the measured currents could be reasonably well fitted, but for the 1:1, 1:5, and 1:15 injection ratios, the fits strongly deviated from the experiment, suggesting the additional existence of heteromeric ASICs that coexist with the homomeric channels within the same cell.

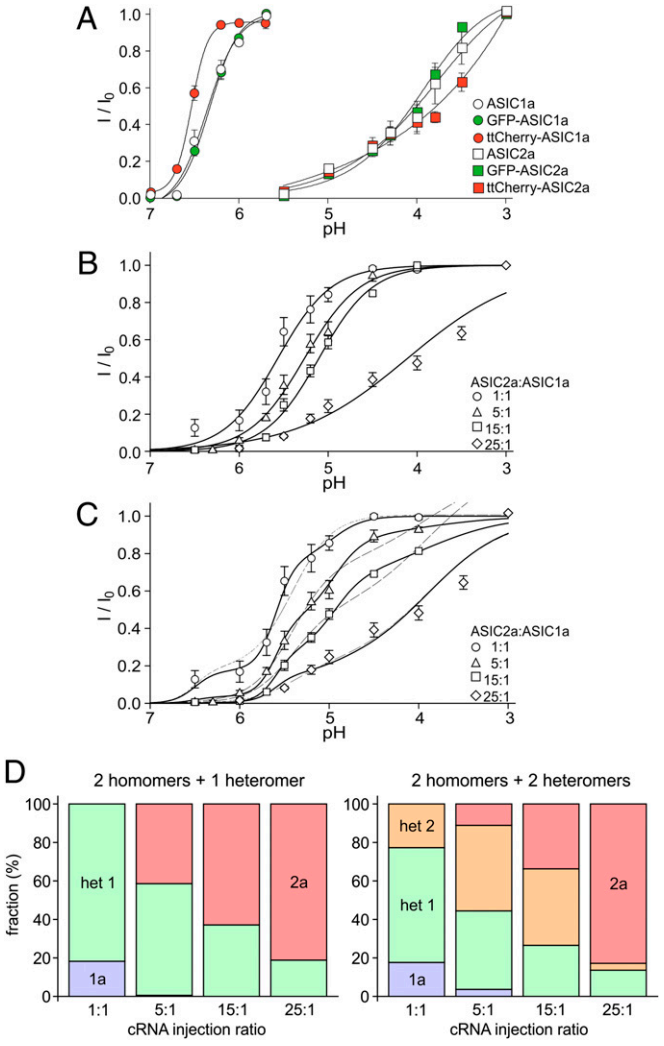

Fig. 1. Electrophysiological characterization of heteromeric ASICs. (*A*) H^+ concentration–response curves of homomeric ASIC1a, ASIC2a, GFP-ASIC1a, and GFP-ASIC2a, respectively, expressed in *Xenopus* oocytes, illustrating identical apparent H^+ affinity of GFP-tagged and untagged ASICs. Lines represent fits to a single Hill function. (*B* and *C*) H^+ concentration–response curves for oocytes expressing ASIC1a and ASIC2a at different ratios. In *B*, lines represent fits to a single Hill function. In *C*, dashed lines represent fits to the sum of three Hill functions: two with the properties of ASIC1a and ASIC2a homomers and one for the ASIC1a/ASIC2a heteromer. Solid lines represent fits of the sum of four Hill functions: two for the ASIC1a and ASIC2a homomers and two for different heteromer species. Data points in *B* and *C* were scaled with different values for I_0 from the Hill curve fits. Error bars in *A*–*C* represent SEM. (*D*) Fractions of homo- and heteromers from the best fits of three (*Left*) or four (*Right*) Hill curves. Absolute current amplitudes are given in Table S1.

Electrophysiology Cannot Discriminate Between Assembly Scenarios. Assuming all ASICs are trimers, two different heteromer compositions are possible, in principle, if ASIC1a and ASIC2a are coexpressed: first, a 2:1 heteromer with two ASIC1a subunits and one ASIC2a subunit; and second, a 1:2 heteromer with one ASIC1a and two ASIC2a. To answer whether we can distinguish between scenarios with a single heteromer or both heteromers, coexisting with homomeric ASICs, we fitted the measured currents to models containing either three or four Hill curves: two with the previously determined ASIC1a and ASIC2a properties, and one or two with free fit parameters that would represent the populations of one or two heteromers, respectively.

The fit of a model with two homomers and one heteromer yielded a H^+ affinity of the heteromer of 5.4 and Hill coefficient of 1.9 (Fig. 1*C*, dashed line). The calculated relative abundances of the ASIC1a homomer, the heteromer, and the ASIC2a homomer shifted from 18%/82%/0% for the 1:1 injection ratio to 0%/19%/81% (25:1) with intermediates of 1%/58%/41% (5:1) and 0%/37%/63% (15:1) (Fig. 1*D* and Table S2).

The fit with four different channel compositions (two homomers, two heteromers) yielded H^+ affinities of the heteromers of 5.6 and 4.9 and Hill coefficients of 4 and 2.5 (Fig. 1*C*, solid line). The relative abundances of the ASIC1a homomer, heteromer 1, heteromer 2, and the ASIC2a homomer were 18%/60%/23%/0% (1:1), 4%/41%/44%/11% (5:1), 0%/27%/40%/34% (15:1) and 0%/14%/4%/83% (25:1), but many of the values displayed large SEs (Fig. 1*D* and Table S2).

Not surprisingly the best fit was obtained in the scenario with two heteromer populations, where we used the largest number of free fit parameters. However, the deviations of the curves from the observed currents were not much bigger in the single heteromer scenario or even in the empirical fit with a single Hill function (Fig. 1*B*). Also the large errors of the relative abundances in the second scenario suggested that the problem of deciding between the two scenarios and finding the relative abundances of homomers and heteromers by electrophysiology is not well posed. We therefore used single-molecule imaging of fluorescently labeled intact ASIC complexes, where the composition of the channels can be directly observed.

Fluorescent Protein Tags Do Not Change the Electrophysiological Properties of ASICs. For single-molecule imaging of the channels, we genetically fused GFP to the cytoplasmic N terminus of ASIC1a and ASIC2a, and assessed a possible impact on channel function by electrophysiological characterization of the fusion proteins. Homomeric ASICs composed of either GFP-ASIC1a or GFP-ASIC2a had properties similar to the parental channels, with complete desensitization and a high H^+ affinity for GFP-ASIC1a, and incomplete desensitization and a low H^+ affinity for GFP-ASIC2a (Fig. 1*A*, Fig. S1, and Table S1). The cRNAs coding for the GFP fusion proteins had to be injected in fivefold higher concentrations to generate currents of amplitudes comparable to the parental channels. To obtain a bright red fluorescent

tag, we fused four copies of mCherry [tandem tetrameric mCherry (ttCherry)] to ASIC1a and ASIC2a. Similar to the fusions of GFP to ASICs, ttCherry-ASIC1a and ttCherry-ASIC2a had electrophysiological properties that were similar to those of ASIC1a and ASIC2a, respectively (Fig. 1*A*, Fig. S1, and Table S1). Compared with GFP fusions, however, cRNAs for ttCherry fusions had to be injected in even higher amounts (16 ng per oocyte).

We then tested whether the electrophysiological properties of heteromeric channels were changed by the fusion tags. We did not systematically compare different ratios of the two cRNAs, but focused on finding a condition which produced a predominantly heteromeric population of ASICs, as for the 5:1 injection ratio of untagged ASICs. Heteromeric ASICs containing one subunit with a GFP fusion, or one with a GFP and the other with a ttCherry fusion, had the same electrophysiological properties as ASICs without GFP (Fig. S3 and Table S3).

Our results suggest that the fusion of GFP or ttCherry to ASIC1a or ASIC2a slowed down their synthesis or transport to the plasma membrane, but did not alter the electrophysiological properties of the channels significantly. Thus, fusion to fluorescent proteins should not affect subunit stoichiometry of ASICs.

Single-Molecule Subunit Counting of Fluorescently Tagged ASICs. In contrast to ensemble-averaging approaches like whole-cell electrophysiology, single-molecule experiments intrinsically resolve distinct subpopulations. Recently we had developed a fluorescence-based single-molecule technique in which we image fluorescent protein-labeled subunits of a membrane protein at very low density at the surface of a living cell, such that individual complexes can be resolved to measure their subunit content and stoichiometry (28). Here we used the method to assess coassembly of red- and green-labeled ASIC1a and ASIC2a and count the number of green-labeled subunits in individual ion channels.

We injected the cRNA of the respective channel subunits into *X. laevis* oocytes, and 18–24h later recorded movies of small membrane areas in a total internal reflection microscopy configuration. The high power of the illuminating lasers bleached the fluorescent tags within a few seconds, enabling us to count the bleaching steps of GFP tags due to their strong and even emission of fluorescent light. Despite its brightness, mCherry bleaches much faster than GFP, which prevented accurate counting of bleaching steps. The ttCherry tag minimizes the chance of missing the emission from the red tag (28, 29).

ASIC1a and ASIC2a Assemble into Homotrimers. Before investigating heteromeric assemblies, we counted the subunits of ASIC1a and ASIC2a homomers. Expression of GFP-ASIC1a or GFP-ASIC2a in *Xenopus* oocytes was adjusted to a membrane density of ≤400 spots in a 25 × 25-μm area, which allowed clear separation of individual molecules (Fig. 2*A*).

In six movies from GFP-ASIC1a expressing cells we identified 1,060 fluorescent spots. Sixty-two percent were immobile and bleached predominantly in two or three steps, and some in a single step. Spots with four bleaching steps were observed only rarely, and none with five or more (Fig. 2*B*). The appearance of discrete bleaching steps indicated that each spot represented a single channel consisting of several GFP-ASIC1a subunits. Because not all GFP tags are fluorescent, the bleaching step number should follow a binomial distribution. Indeed, when we performed a least-squares fit assuming a trimeric composition of the GFP-ASIC1a channel with the probability P of GFP to be fluorescent as a free parameter, we obtained a good fit with $P = 78\%$, virtually identical to previous results (Fig. 2*C*) (28). A very similar picture emerged when counting the subunits of GFP-ASIC2a. Of 871 spots from three oocytes, 52% were immobile and displayed well-behaved bleaching steps, and the distribution of bleaching steps was well fitted by a binomial distribution for a trimer and $P = 77\%$ (Fig. 2*D*).

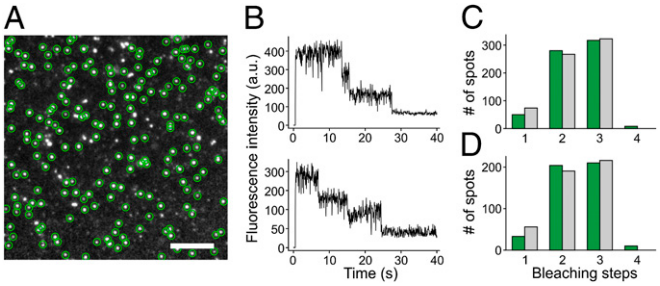

Fig. 2. Single-molecule subunit counting of homomeric GFP-ASIC1a and GFP-ASIC2a. (*A*) Image from a TIRF movie with GFP-ASIC1a expressed at the cell surface of a *X. laevis* oocyte. Green circles indicate immobile spots suitable for counting of bleaching steps. (Scale bar: 5 μm.) (*B*) Fluorescence intensity from two GFP-ASIC1a spots exemplary of a three-step photobleaching process. (*C* and *D*) The distribution of observed bleaching steps (green bars) for (*C*) GFP-ASIC1a and (*D*) GFP-ASIC2a and fits of binomial distributions (gray bars).

Events with four bleaching steps, which should never appear for a trimeric protein, can be explained by the coincidental overlap of two spots within a diffraction-limited volume. When excluding this artifact, the confidence level that the observed distribution originates from a trimeric assembly is very close to 100% with a sample size >100 for a fluorescence probability of $P > 75\%$ (30). Therefore, our data confirm the notion that ASIC1a and ASIC2a, when expressed alone, assemble into homotrimers (12, 25).

Coexpression of Green- and Red-Labeled ASIC Subunits. Our aim was to decide whether ASIC1a and ASIC2a can assemble in both 1:2 and 2:1 heteromeric compositions, and to deduce the fractions of 0:3, 1:2, 2:1, and 3:0 homo- and heteromers. For this purpose we coexpressed GFP- and ttCherry-labeled ASIC1a and ASIC2a subunits, colocalized red and green fluorescence at the single-molecule level, and counted the GFP bleaching steps.

The calculation of homo- and heteromer fractions is complicated by the fact that a sizeable fraction of green and red tags is nonfluorescent. For example, a heteromeric channel carrying tags of both colors could appear only green when the red tags are not functional, or only red when the green tags are not functional. A trimeric channel can carry functional and nonfunctional green and red fluorescent proteins in 20 different ways (Fig. 3*A*). The relative occurrences of these combinations can be calculated from the fractions of homo- and heteromers and the probabilities for GFP and ttCherry to be functional (*Materials and Methods*). Accordingly, it is possible by least-squares fitting to reconstruct the fractions of homo- and heteromers from the observed red/green overlap and bleaching steps (Fig. 3*B*).

To test this strategy, we first used a mix of GFP- and ttCherry-labeled ASIC1a because they should assemble in a completely random fashion. After that, we proceeded to differentially tagged ASIC1a and ASIC2a.

Green- and Red-Tagged ASIC1a Subunits Assemble Randomly into Trimers. We coexpressed GFP-ASIC1a with ttCherry-ASIC1a and titrated the amount of coinjected RNA to obtain comparable surface densities of green and red fluorescent spots. For the movie acquisitions, we first excited and imaged ttCherry for ∼2 s (sufficient to bleach the majority of red spots) and then GFP for further ∼30 s (long enough to bleach most green spots). The first five images of green and red emission were overlaid to identify colocalization of GFP-ASIC1a and ttCherry-ASIC1a (Fig. 4*A*). Bleaching steps from immobile spots were counted in the green channel (Fig. 4*B*).

We collected 2,692 spots from a total of 13 movies, and determined the green/red overlap and counted the bleaching steps in the green channel (Fig. 4*C*). Thirty-seven percent of the spots

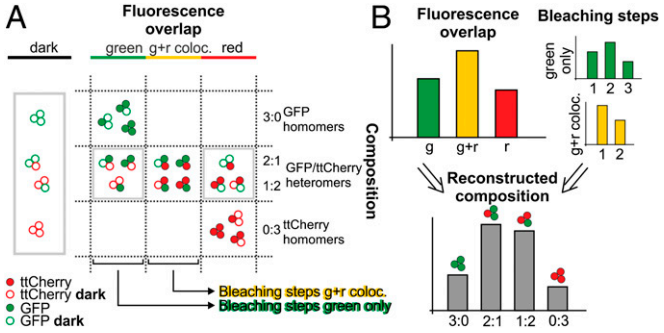

Fig. 3. Principle of assembly of red- and green-tagged subunits into homo- and heteromers. (*A*) Recorded fluorescence from single channels is green, red, or a colocalization of green and red, depending on the channel composition and the functionality of the tags. When none of the tags is functional, channels stay dark (*Left*). For certain channels, the fluorescence does not reflect the composition (gray boxes). Of channels with functional GFP tags, the bleaching steps can be counted. (*B*) From the observed distribution of green-only, red-only, and colocalized spots and the bleaching steps, the underlying fractions of homo- and heteromeric channels can be reconstructed.

were fluorescent only in green, 23% only in red, and 40% in both colors. Of the green-only spots, 93% had clear bleaching steps, of which 30% bleached in one, 50% in two, 20% in three steps, and no spots had four bleaching steps. Of the spots that had green and red fluorescence, 87% had clear bleaching steps in the green channel; 60% of those had one, 39% two, and 1.5% three steps (all numbers summarized in Table S4).

To obtain estimates of homo- and heteromer fractions, we used least-squares fitting with the fractions of homo- and heteromeric assemblies with green:red content of 3:0, 2:1, 1:2, and 0:3 as free parameters (*Materials and Methods*). Also the probability of the red tag being fluorescent was used as free parameter, whereas the probability of GFP being fluorescent was kept at 78%, the value we had determined above and in earlier work (28). The fit yielded fractions of 16% for GFP-ASIC1a homomers (3g:0r, where g represents green subunits and r represents red subunits), 19% for ttCherry-ASIC1a homomers (0g:3r), 43% for heteromers containing two GFP-ASIC1a and one ttCherry-ASIC1a (2g:1r), and 23% for heteromers containing one GFP-ASIC1a and two ttCherry-ASIC1a (1g:2r) (Fig. 4*D*).

A model of random mixing between green- and red-labeled ASIC1a subunits, without a preference for any homo- or heteromeric combination of subunits, would imply a binomial relationship between the four assemblies with a single free parameter, namely the ratio of green to red subunits. We repeated the fit under this assumption and again obtained a good match of the fit to the counted spots (Fig. 4*E*). The fit yielded fractions of 18% for 3g:0r, 41% for 2g:1r, 32% for 1g:2r, and 8% for 0g:3r channels (Fig. 4*F*).

The distributions of homo- and heteromers reconstructed from the two fits were similar except for a ~10% higher fraction of ttCherry-ASIC1a homomers on the cost of a smaller fraction of 1g:2r heteromers when the model with four independent fractions was used for fitting (Fig. 4 *D* and *F*). The similarity confirms that by fitting colocalization and bleaching step information simultaneously while using the four fractions of 3:0, 2:1, 1:2, and 0:3 homo- and heteromers as free parameters, we could approximately reconstruct the binomial distribution of randomly mixed GFP-ASIC1a and ttCherry-ASIC1a. The small bias toward more red-only spots was likely introduced by excluding a larger fraction of GFP-containing spots due to movement. Red spots bleached much faster than green spots, making the detection of movement in the red channel less likely.

To confirm that the number of spots we counted was large enough to lead to significant results of the fits, we performed Monte Carlo simulations with different fractions for homo- and heteromers. With 2,000 simulated spots, the fit values for homo- and heteromer fractions were within 2.5% of the input values (Fig. S4). The low deviation between fit and input values suggested that evaluation of 2,000 spots would result in a significant representation of the underlying homo- and heteromer fractions.

Labeled ASIC1a and ASIC2a Assemble Randomly into Coexisting Homo- and Heterotrimers. After the experimental validation that green- and red-tagged ASIC1a subunits assemble randomly to homotrimers, we wanted to determine the fractions of homo- and heteromers that form when ASIC1a and ASIC2a are being coexpressed.

We expressed GFP-ASIC1a and ttCherry-ASIC2a at comparable surface densities, and used the same imaging protocol as in

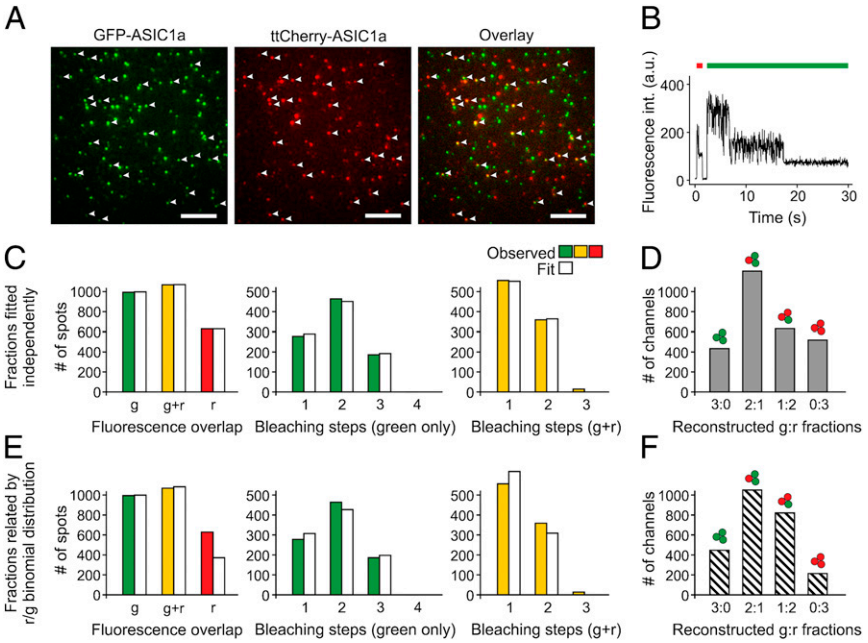

Fig. 4. Assembly of differentially tagged ASIC1a subunits. (*A*) Microscope image of an oocyte patch with GFP-ASIC1a and ttCherry-ASIC1a. Arrowheads mark colocalized GFP and ttCherry spots. (Scale bars: 5 μm.) (*B*) Fluorescence intensity profile over time from a representative colocalized spot. ttCherry was excited first (red bar) followed by GFP (green bar). In-between, lasers are off and the intensity drops to zero. (*C*) Histograms for observed spots with green-only, red-only, and colocalized green and red fluorescence, and for GFP bleaching steps of green-only spots and of spots where green and red colocalized. All four fractions of homo- and heteromers were used as free parameters. Filled bars indicate the observed distribution and white bars are the results of the least-squares fit. (*D*) Fitted fractions of homo- and heteromeric channels of stoichiometry are as indicated. (*E*) Experimental histograms were fitted with homo- and heteromer ratios as given by a binomial distribution, with the ratio of ASIC2a to ASIC1a as a free parameter. (*F*) Reconstructed fractions of homo- and heteromers.

the GFP-ASIC1a/ttCherry-ASIC1a coexpression experiment. First, ttCherry was imaged and bleached, and then GFP, allowing us to count the GFP bleaching steps. From the overlay of green and red emission we identified spots where GFP and ttCherry emission colocalized (Fig. S5*A*). Many of the immobile spots displayed clear bleaching steps in the green channel (Fig. S5*B*).

We collected 2,418 spots from 12 movies recorded from four different batches of oocytes. Thirty percent of the spots were fluorescent only in green, 21% only in red, and 50% in both colors (Fig. 5*A*). Ninety two percent of the green-only spots had clear bleaching steps, and of those, 39% bleached in one, 45% in two, and 16% in three steps, and no spots with four bleaching steps were found. Of the spots that had green and red fluorescence, 85% had clear bleaching steps, and 64% of them were bleached in one, 35% in two, and 1% in three steps (Table S4).

The least-squares fit where we kept all fractions of homo- and heteromers as free parameters yielded 9% for GFP-ASIC1a homomers (3g:0r), 13% for ttCherry-ASIC2a homomers (0g:3r), 45% for heteromers containing two GFP-ASIC1a and one ttCherry-ASIC2a (2g:1r), and 33% for heteromers containing one GFP-ASIC1a and two ttCherry-ASIC2a (1g:2r) (Fig. 5*B*). The same data fitted with a model where homo- and heteromer fractions are related via a binomial distribution—implying random assembly of GFP-ASIC1a and ttCherry-ASIC2a—yielded 13% for 3g:0r homomers, 12% for 0g:3r homomers, 38% for 2g:1r heteromers, and 37% for 1g:2r heteromers (Fig. 5*B*).

Next, to investigate whether exchanging the green and red tags on the ASIC1a and ASIC2a subunits would lead us to the same results, we coexpressed GFP-ASIC2a and ttCherry-ASIC1a. Again, we observed colocalization of red and green fluorescent spots with clear bleaching steps in the green channel (Fig. S5 *C* and *D*). Of 2,264 spots from 12 movies and 2 different batches of oocytes, 28% spots showed only green, 20% only red, and 52% green and red fluorescence (Fig. 5*C*). Of the green-only spots, 89% had clear bleaching steps, of which 36% were bleached in one, 41% in two, and 23% in three steps, and there were no spots in four steps. Of the green and red spots, 83% had clear bleaching steps, and 69% were bleached in one, 30% in two, and 1% in three steps (Table S4).

The evaluation was performed as in the previous experiment. The fit yielded fractions of 12% for GFP-ASIC2a homomers (3g:0r), 11% for ttCherry-ASIC1a homomers (0g:3r), 37% for heteromers containing two GFP-ASIC2a and one ttCherry-ASIC1a (2g:1r), and 39% for heteromers containing one GFP-ASIC2a and two ttCherry-ASIC1a (1g:2r) (Fig. 5*D*). The same data fitted with a binomial distribution model yielded 12% for 3g:0r homomers, 13% for 0g:3r homomers (0:3), 37% for 2g:1r heteromers, and 38% for 1g:2r heteromers (Fig. 5*D*).

The significant overlap of green and red fluorescent spots supports the evidence obtained from electrophysiology that ASIC1a and ASIC2a form heteromeric channels in *Xenopus* oocytes. The fit with independent fractions of homo- and heteromers suggests that both ASIC1a/ASIC2a heteromeric assemblies with 2:1 and 1:2 compositions can form and coexist with the 3:0 and 0:3 homomers. Beyond that, the close match of the fit with independent fractions and the fit with a binomial relation between the homo- and heteromer fractions demonstrates that GFP-ASIC1a and ttCherry-ASIC2a subunits, as well as GFP-ASIC2a and ttCherry-ASIC1a subunits, mix randomly, without a preference to form either one of the homo- or heteromeric assemblies.

Discussion

This study has two major findings: First, we could confirm the trimeric structure of homomeric ASIC1a and ASIC2a in the plasma membrane of living cells; and second, we resolved for the first time, to our knowledge, the stoichiometry of a heteromeric ASIC, showing that it is flexible and that heterotrimeric ASIC1a/ASIC2a can contain either two ASIC1a or two ASIC2a subunits. Moreover, we provide compelling evidence that ASIC1a and ASIC2a assemble randomly into heteromers, so that heteromeric channels have no preferred composition.

The electrophysiological data clearly demonstrated the formation of ASIC1a/2a heteromers and their coexistence with either ASIC1a or ASIC2a homomers within the same cell (Fig. 1*C*). The coexistence of homo- and heteromeric channels with distinct electrophysiological characteristics complicates a straightforward determination of the heteromer stoichiometry with population-based methods like whole-cell electrophysiology.

To overcome these problems, we complemented our studies with the single-molecule photobleaching approach (28). This technique provides three main opportunities. First, the use of differentially fluorescent protein-tagged subunits unambiguously proves or disproves their interaction; second, the bleaching steps of GFP resolve the subunit content of a complex; and third, as a quantitative approach, it tracks also small subpopulations of channels, regardless of their functionality.

Coexpression of differentially fluorescent protein-tagged ASIC1a and ASIC2a yielded a significant red/green overlap, indicating the existence of heteromeric channels (Fig. S5). Moreover, the combination of colocalization and GFP-bleaching step analysis unraveled a flexible 2:1/1:2 stoichiometry of the heteromers, and ASIC1a and ASIC2a appear to coassemble in a completely random fashion. The single-molecule approach clearly showed that both heteromers coexisted with both homomers (ASIC1a and ASIC2a) within the same cell.

The domains that govern ASIC subunit assembly are largely unknown. It has been shown for other ion channels, for example

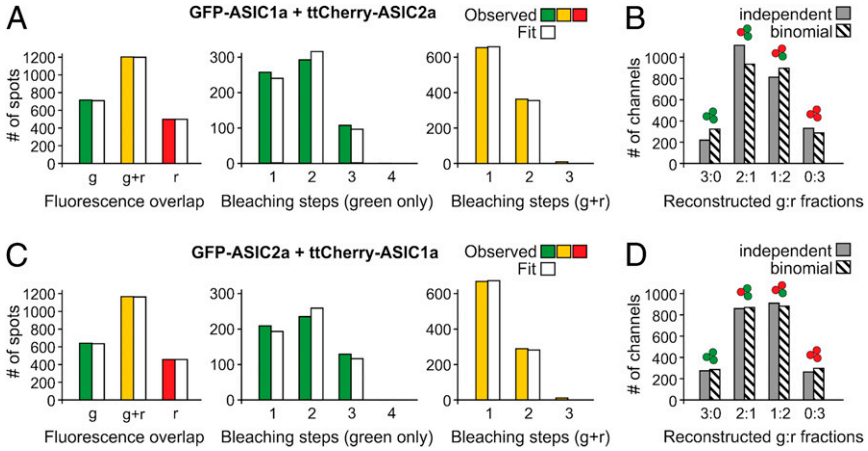

Fig. 5. Assembly of ASIC1a/2a heteromers. (*A*) Histograms for counted spots of GFP-ASIC1a/ttCherry-ASIC2a with the properties as indicated and the fit values. (*B*) Fit for fractions of homo- and heteromers with independent fractions and fractions related by a binomial distribution, implying random assembly. (*C*) Histograms for counted spots of GFP-ASIC2a/ttCherry-ASIC1a with the properties as indicated and the fit values. (*D*) Fit for fractions of homo- and heteromers with independent fractions and fractions related by a binomial distribution.

glutamate receptors, that assembly is governed by high-affinity interactions of specific domains on the individual subunits (31). Therefore, ion channel stoichiometry should be independent of the expression system. We cannot rule out, however, that in a mammalian neuron, chaperones assist in ASIC assembly and bias the intrinsically random assembly of ASIC1a and ASIC2a to favor a particular subunit composition. Therefore, in the future, the existence of two different ASIC1a/2a heteromers has to be confirmed in neurons. The ASIC1a/2a heteromer is one of the major ASICs in the brain; the existence of ASIC1a/2a heteromers with two different compositions indicates that the variety of ASICs in the central nervous system might be greater than previously thought. For hippocampal neurons and dorsal horn neurons it has been specifically shown that heteromeric ASIC1a/2a channels coexist with homomeric ASIC1a in a large fraction of neurons (3–6, 32). The coexistence with homomeric ASIC2a was not documented because the most acidic pH tested was 5.0, which will not substantially activate homomeric ASIC2a due to its low H^+ affinity. Similar to our own results, one study found that functional properties of heteromeric ASIC1a/2a shift depending on the ratio of DNAs transfected into COS cells (32). Based on the similarity of currents at a 2:1 ratio (ASIC1a/ASIC2a) with endogenous currents of spinal horn neurons, it was concluded that heteromeric ASICs in spinal horn neurons have a 2:1 (ASIC1a/ASIC2a) stoichiometry. Another study found that functional properties of ASICs in cortical neurons continuously shift during development paralleling a continuously increasing ratio of ASIC2a/ASIC1a mRNA (33). These studies suggest that the ratio of ASIC1a/ASIC2a mRNA levels continuously shift the properties of native ASICs and that neurons of the central nervous system mainly use ASIC2a expression levels to fine-tune the properties of their ASICs. Because it has been proposed that ASIC2a facilitates localization of ASIC1a in dendritic spines (34), the formation of heteromeric assemblies might have even more profound implications beyond the fine-tuning of functional properties.

Most heteromeric ion channels have a fixed stoichiometry (35). Thus, it is possible that other heteromeric ASICs, like the ASIC1a/2b (7) or the ASIC3/2b (36, 37) heteromer, do not have a flexible but fixed stoichiometry. The elucidation of the stoichiometry of these ASICs is therefore another pressing question that needs to be addressed in the future.

Materials and Methods

Electrophysiology. Animal care and experiments followed approved institutional guidelines at the Universities of Aachen and Freiburg. cRNA from untagged, GFP-, or ttCherry-tagged ASIC1a and ASIC2a was generated by in vitro transcription and injected into *Xenopus* oocytes. Two to 4 d later, whole-cell currents were recorded by two-electrode voltage clamp with a fast perfusion system.

Single-Molecule Imaging. Oocytes expressing fluorescent protein-tagged ASIC constructs were devitellinized and imaged on an Olympus IX71 microscope in total internal reflection fluorescence (TIRF) mode (28). Emission from single molecules was recorded with an EMCCD camera (Andor). Bleaching steps in the emission were counted manually.

For a complete description of the materials and methods used, see *SI Materials and Methods*.

ACKNOWLEDGMENTS. This work was supported by Deutsche Forschungsgemeinschaft Grant GR1771/3-5 (to S.G.) and the Excellence Initiative of the German Federal and State Governments (EXC 294).

1. Gründer S, Chen X (2010) Structure, function, and pharmacology of acid-sensing ion channels (ASICs): Focus on ASIC1a. *Int J Physiol Pathophysiol Pharmacol* 2(2):73–94.
2. Wemmie JA, et al. (2002) The acid-activated ion channel ASIC contributes to synaptic plasticity, learning, and memory. *Neuron* 34(3):463–477.
3. Baron A, Waldmann R, Lazdunski M (2002) ASIC-like, proton-activated currents in rat hippocampal neurons. *J Physiol* 539(Pt 2):485–494.
4. Askwith CC, Wemmie JA, Price MP, Rokhlina T, Welsh MJ (2004) Acid-sensing ion channel 2 (ASIC2) modulates ASIC1 H+-activated currents in hippocampal neurons. *J Biol Chem* 279(18):18296–18305.
5. Vukicevic M, Kellenberger S (2004) Modulatory effects of acid-sensing ion channels on action potential generation in hippocampal neurons. *Am J Physiol Cell Physiol* 287(3):C682–C690.
6. Wu LJ, et al. (2004) Characterization of acid-sensing ion channels in dorsal horn neurons of rat spinal cord. *J Biol Chem* 279(42):43716–43724.
7. Sherwood TW, Lee KG, Gormley MG, Askwith CC (2011) Heteromeric acid-sensing ion channels (ASICs) composed of ASIC2b and ASIC1a display novel channel properties and contribute to acidosis-induced neuronal death. *J Neurosci* 31(26):9723–9734.
8. Wu PY, et al. (2013) Acid-sensing ion channel-1a is not required for normal hippocampal LTP and spatial memory. *J Neurosci* 33(5):1828–1832.
9. Xiong ZG, et al. (2004) Neuroprotection in ischemia: Blocking calcium-permeable acid-sensing ion channels. *Cell* 118(6):687–698.
10. Friese MA, et al. (2007) Acid-sensing ion channel-1 contributes to axonal degeneration in autoimmune inflammation of the central nervous system. *Nat Med* 13(12):1483–1489.
11. Diochot S, et al. (2012) Black mamba venom peptides target acid-sensing ion channels to abolish pain. *Nature* 490(7421):552–555.
12. Jasti J, Furukawa H, Gonzales EB, Gouaux E (2007) Structure of acid-sensing ion channel 1 at 1.9 A resolution and low pH. *Nature* 449(7160):316–323.
13. Chen X, Kalbacher H, Gründer S (2006) Interaction of acid-sensing ion channel (ASIC) 1 with the tarantula toxin psalmotoxin 1 is state dependent. *J Gen Physiol* 127(3):267–276.
14. Baconguis I, Gouaux E (2012) Structural plasticity and dynamic selectivity of acid-sensing ion channel-spider toxin complexes. *Nature* 489(7416):400–405.
15. Dawson RJ, et al. (2012) Structure of the acid-sensing ion channel 1 in complex with the gating modifier Psalmotoxin 1. *Nat Commun* 3:936.
16. Gründer S, Augustinowski K (2012) Toxin binding reveals two open state structures for one acid-sensing ion channel. *Channels (Austin)* 6(6):409–413.
17. Gao Y, et al. (2007) Fluorescence resonance energy transfer analysis of subunit assembly of the ASIC channel. *Biochem Biophys Res Commun* 359(1):143–150.
18. Firsov D, Gautschi I, Merillat AM, Rossier BC, Schild L (1998) The heterotetrameric architecture of the epithelial sodium channel (ENaC). *EMBO J* 17(2):344–352.
19. Kosari F, et al. (1998) Subunit stoichiometry of the epithelial sodium channel. *J Biol Chem* 273(22):13469–13474.
20. Dijkink L, Hartog A, van Os CH, Bindels RJ (2002) The epithelial sodium channel (ENaC) is intracellularly located as a tetramer. *Pflugers Arch* 444(4):549–555.
21. Anantharam A, Palmer LG (2007) Determination of epithelial Na+ channel subunit stoichiometry from single-channel conductances. *J Gen Physiol* 130(1):55–70.
22. Snyder PM, Cheng C, Prince LS, Rogers JC, Welsh MJ (1998) Electrophysiological and biochemical evidence that DEG/ENaC cation channels are composed of nine subunits. *J Biol Chem* 273(2):681–684.
23. Eskandari S, et al. (1999) Number of subunits comprising the epithelial sodium channel. *J Biol Chem* 274(38):27281–27286.
24. Staruschenko A, et al. (2004) Fluorescence resonance energy transfer analysis of subunit stoichiometry of the epithelial Na+ channel. *J Biol Chem* 279(26):27729–27734.
25. Gonzales EB, Kawate T, Gouaux E (2009) Pore architecture and ion sites in acid-sensing ion channels and P2X receptors. *Nature* 460(7255):599–604.
26. Carnally SM, et al. (2008) Direct visualization of the trimeric structure of the ASIC1a channel, using AFM imaging. *Biochem Biophys Res Commun* 372(4):752–755.
27. Bassilana F, et al. (1997) The acid-sensitive ionic channel subunit ASIC and the mammalian degenerin MDEG form a heteromultimeric H+-gated Na+ channel with novel properties. *J Biol Chem* 272(46):28819–28822.
28. Ulbrich MH, Isacoff EY (2007) Subunit counting in membrane-bound proteins. *Nat Methods* 4(4):319–321.
29. Jain A, et al. (2011) Probing cellular protein complexes using single-molecule pull-down. *Nature* 473(7348):484–488.
30. Hines KE (2013) Inferring subunit stoichiometry from single molecule photobleaching. *J Gen Physiol* 141(6):737–746.
31. Kumar J, Schuck P, Mayer ML (2011) Structure and assembly mechanism for heteromeric kainate receptors. *Neuron* 71(2):319–331.
32. Baron A, Voilley N, Lazdunski M, Lingueglia E (2008) Acid sensing ion channels in dorsal spinal cord neurons. *J Neurosci* 28(6):1498–1508.
33. Li M, Kratzer E, Inoue K, Simon RP, Xiong ZG (2010) Developmental change in the electrophysiological and pharmacological properties of acid-sensing ion channels in CNS neurons. *J Physiol* 588(Pt 20):3883–3900.
34. Zha XM, et al. (2009) ASIC2 subunits target acid-sensing ion channels to the synapse via an association with PSD-95. *J Neurosci* 29(26):8438–8446.
35. Barrera NP, Edwardson JM (2008) The subunit arrangement and assembly of ionotropic receptors. *Trends Neurosci* 31(11):569–576.
36. Lingueglia E, et al. (1997) A modulatory subunit of acid sensing ion channels in brain and dorsal root ganglion cells. *J Biol Chem* 272(47):29778–29783.
37. Sutherland SP, Benson CJ, Adelman JP, McCleskey EW (2001) Acid-sensing ion channel 3 matches the acid-gated current in cardiac ischemia-sensing neurons. *Proc Natl Acad Sci USA* 98(2):711–716.